This article has been accepted for publication in a future issue of this journal, but has not been fully edited. Content may change prior to final publication. Citation information: DOI 10.1109/TAP.2020.2975534, IEEE Transactions on Antennas and Propagation

Millimeter-Wave Dual-Polarized Filtering Antenna for 5G Application

Sheng Jie Yang, Yong Mei Pan, *Senior Member, IEEE*, Li-Yun Shi, and Xiu Yin Zhang, *Senior Member, IEEE*[1]

***Abstract*—This paper presents a novel dual-polarized millimeter-wave (mm-Wave) patch antenna with bandpass filtering response. The proposed antenna consists of a differential-fed cross-shaped driven patch and four stacked parasitic patches. The combination of the stacked patches and the driven patch can be equivalent to a bandstop filtering circuit for generating a radiation null at the upper band-edge. Besides, four additional shorted patches are added beside the cross-shaped driven patch to introduce another radiation null at the lower band-edge. Moreover, by embedding a cross-shaped strip between these four stacked patches, the third radiation null is generated to further suppress the upper stopband. As a result, a quasi-elliptic bandpass response is realized without requiring extra filtering circuit. For demonstration, a prototype was fabricated with standard PCB process and measured. The prototype operates in the 5G band (24.25−29.5 GHz) and it has an impedance bandwidth of 20%. The out-of-band gain drops over 15 dB at 23 GHz and 32.5 GHz respectively, which exhibits high-selectivity. These merits make the proposed antenna a good element candidate for the 5G mm-Wave massive MIMO applications to reduce the requirements of the filters in the mm-Wave RF frontends.**

***Index Terms*—Filtering antenna, millimeter-wave antenna, dual-polarized antenna.**

I. Introduction

WITH the advantages such as wide bandwidth, high data rate, and low latency, the millimeter-wave (mm-Wave) communication has attracted extensive attention in 5G applications [1]. In 5G mm-Wave front-ends, filters are usually needed to suppress the unwanted image frequency spectrum, LO leakage and harmonics. However, compact on-chip filters [2]−[4] feature the low-quality (Q)-factor, resulting in a high insertion loss which is generally over 2.5 dB. Besides, the high-Q filters [5]−[6] are not easy to be integrated in 5G mm-Wave system due to the large size. Moreover, if the high-Q filter is packaged separately, the interconnection between the filter and the chip is required, which will also cause high insertion loss in the mm-Wave band. In order to solve this problem, an effective solution is to integrate filtering response into the antenna to realize the so-called filtering antenna, and thus to simplify the design of filters in the mm-Wave RF frontends to a certain extent.

A typical method of designing a filtering antenna is to incorporate filtering circuits into feeding networks [7]−[14]. This method is straightforward. But, still, the insertion loss of the additional filtering circuits is unavoidable. As an alternative, specific parasitic elements, such as parasitic patch [15]−[17], slot [18]−[20], shorting pins [21], microstrip stub [22], and metallic loop [23] were used in antennas, to generate radiation nulls beside the operating passband so as to realize the filtering function. In this way, no extra filtering circuit is required, leading to lower insertion loss and more compact size.

A number of filtering antennas have been developed in the last decade by the above two methods [7]−[24]. However, thus far, most of them operate at microwave frequency band. In addition, due to the limitation of mm-Wave processing technology, not all of them are suitable to be designed at mm-Wave frequency (e.g. the dipole antenna in [23] is difficult to be assembled at the high frequency). Recently, a few mm-Wave filtering antennas were realized based on substrate integrated waveguide (SIW) filters [11]−[14]. These antennas exhibit high-Q filtering response and good frequency selectivity. But, unfortunately, they generally suffer from narrow bandwidth (less than 5%), which is not sufficient for specific wideband applications. Besides, due to the integration of SIW filter, some of them feature bulky size. For example, the Ka-band single-polarized SIW filtering antenna in [12] occupies a large size of $0.92 \times 1\ \lambda_c^2$ (λ_c denotes the wavelength at the central frequency of the passband), and the dual-polarized design in [14] takes up a larger size of $1.73 \times 1.73\ \lambda_c^2$. Therefore, they are not suitable to be used as an antenna element in the 5G mm-Wave massive MIMO arrays, in which the element spacing is usually less than 0.5 λ_c for wide-angle scanning.

In this paper, an mm-Wave wideband dual-polarized filtering microstrip antenna is proposed. It mainly consists of a differential-fed cross-shaped driven patch and four stacked parasitic patches. In addition, four shorted patches are added at the corners of the cross-shaped driven patch to generate a radiation null at the lower stopband, whereas a cross-shaped strip is introduced between the four stacked parasitic patches to realize an extra radiation null at the higher stopband. As a result, a bandpass filtering response with sharp roll-off rate is achieved.

Manuscript received November 7, 2019.

This work was supported in part by National Key Research and Development Program of China under Grant 2018YFB1801601 and in part by National Natural Science Foundation of China under Grants 61725102 and in part by Science and Technology Program of Guangzhou Development District, China, under Grant 2018GH10. (*Corresponding author: Xiu Yin Zhang*)

S.-J. Yang, Y.-M. Pan and X.-Y. Zhang are with the School of Electronic and Information Engineering, South China University of Technology, Guangzhou, 510641, China (e-mail: zhangxiuyin@scut.edu.cn).

L.-Y. Shi is with the School of Electronic Information and Electrical Engineering, Shanghai Jiao Tong University, Shanghai, China.

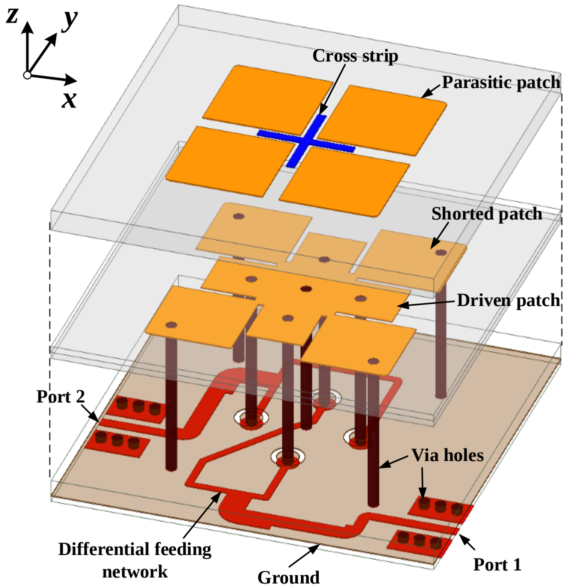

Fig. 1. Geometry stack-up of the proposed dual-polarized filtering antenna.

The proposed filtering antenna has a compact size, which is suitable for 5G mm-Wave massive MIMO applications. The working mechanism, design guideline, as well as measured results of the proposed antenna are presented in the following sections.

II. Antenna Configuration and Working Mechanism

A. Antenna Configuration

Fig. 1 and Fig. 2 illustrate the configuration of the proposed dual-polarized filtering antenna, and the specific dimensions of the antenna are listed in Table I. It is composed of parasitic patches, driven patch, ground plane and differential feeding networks. In order to reduce the fabrication cost, a standard PCB process is adopted. As shown in Fig. 2(a), the entire structure consists of three laminates (Sub 1: Rogers 4003C with a thickness of 305um; Sub 3: Rogers 4350B with a thickness of 102um; Sub 5: Rogers 4350B with a thickness of 102um), two bondply layers (Sub 2: Rogers 4450F with a thickness of 102um; Sub 4: Rogers 4450F with a thickness of 305um) and 4 metal layers (a copper thickness of 18um). The four parasitic patches together with a cross-shaped strip are printed on metal Layer 1, and the driven patch together with four additional shorted patches are printed on metal Layer 2, as shown in Fig. 2(b) and Fig. 2(c), respectively. The ground plane and feeding networks of the antenna are fabricated on metal Layer 3 and Layer 4 separately. With reference to Fig. 2(d), the two-port differential feeding networks are located under the ground to excite the driven patch through via holes. The main function of the differential feeding networks in the proposed antenna is to enhance the isolation between the two ports and the cross-polarization discrimination (XPD).

B. . Antenna Mechanism

To better illustrate the mechanism of the proposed filtering antenna, three reference designs are investigated, as shown in Fig. 3. For simplicity, the differential feeding networks are removed, and a pair of ideal differential ports (Port 1^+ and Port 1^-) are used in the reference antennas. The corresponding

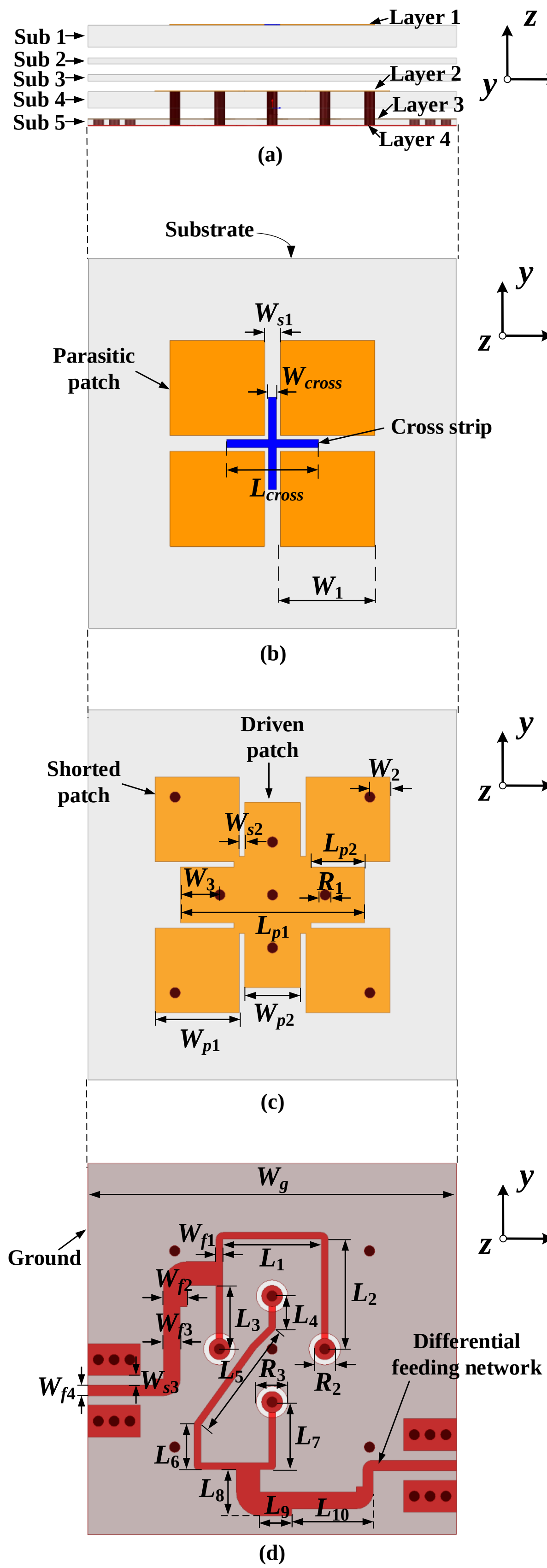

Fig. 2. Configuration of the dual-polarized filtering antenna. (a) The lamination stack-up of the antenna package. (b) Top view of the parasitic patches. (c) Top view of the driven patch. (d) Top view of the differential feeding networks.

This article has been accepted for publication in a future issue of this journal, but has not been fully edited. Content may change prior to final publication. Citation information: DOI 10.1109/TAP.2020.2975534, IEEE Transactions on Antennas and Propagation

TABLE I
PARAMETERS OF THE PROPOSED FILTERING ANTENNA

Length	L_1	L_2	L_3	L_4	L_5	L_6	L_7
Value (mm)	1.87	2.07	1.2	0.65	2.27	0.71	1.28
Length	L_8	L_9	L_{10}	L_{p1}	L_{p2}	L_{cross}	W_1
Value (mm)	0.87	0.6	1.55	3.5	1.02	1.75	1.8
Length	W_2	W_3	W_{p1}	W_{p2}	W_{f1}	W_{f2}	W_{f3}
Value (mm)	0.38	0.75	1.6	1.06	0.13	0.45	0.32
Length	W_{f4}	W_{s1}	W_{s2}	W_{s3}	W_{cross}	W_g	R_1
Value (mm)	0.2	0.3	0.1	0.18	0.15	7	0.2
Length	R_2	R_3					
Value (mm)	0.4	0.6					

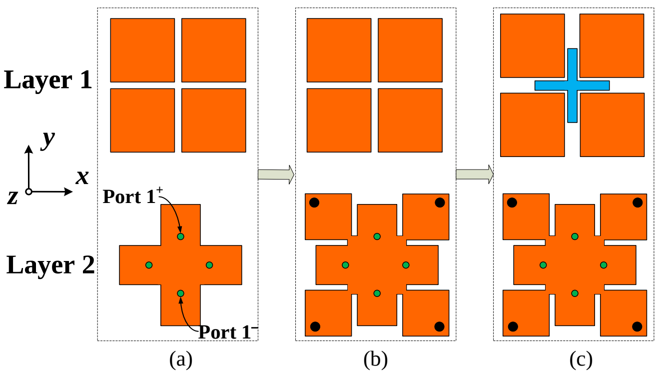

Fig. 3. Top views of different reference antennas. (a) Design I. (b) Design II. (c) Design III.

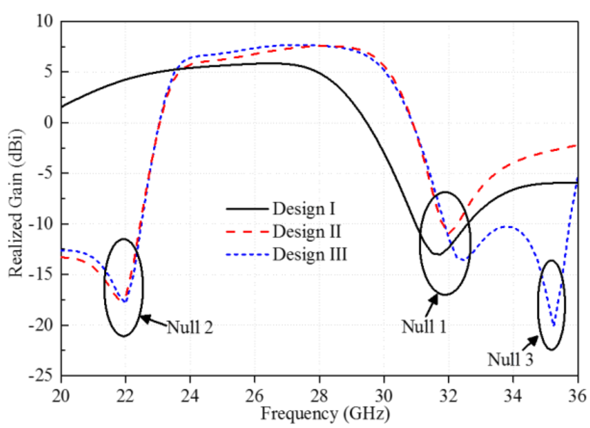

Fig. 4. Simulated realized gains of different reference antennas.

simulated realized gains of these antennas are depicted in Fig. 4. In reference Design I, a cross-shaped driven patch along with four stacked parasitic patches can introduce a radiation null at around 32 GHz (Null 1), enhancing the roll-off rate at the edge of the higher stopband (see the black solid line in Fig. 4). By adding four extra shorted patches around the cross-shaped driven patch, reference Design II is obtained, and another radiation null (Null 2) is generated at the lower band-edge (see the red dash line in Fig. 4). In reference Design III, a cross-shaped strip is embedded between the four stacked patches, which generates a third radiation null (Null 3) to

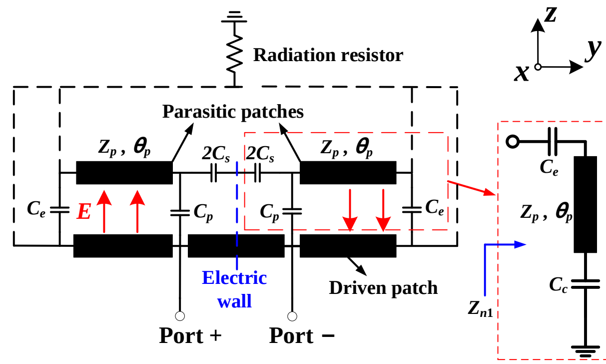

Fig. 5. The equivalent circuit model for reference Design I.

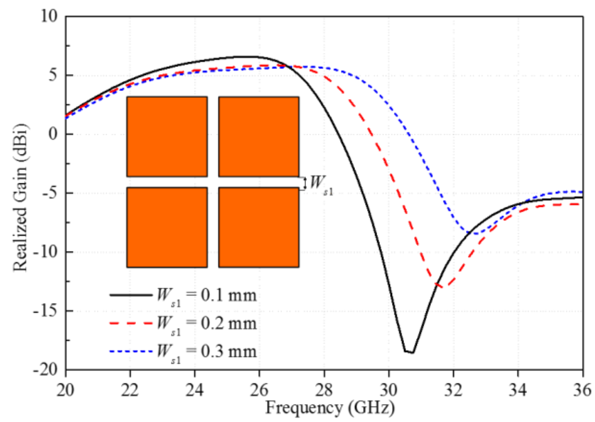

Fig. 6. Simulated realized gains of reference Design I for different W_{s1}.

further suppress the upper stopband (see the blue dash line in Fig. 4). Consequently, a quasi-elliptic bandpass response is realized with the aid of these three radiation nulls. The generative mechanisms of Null 1 − Null 3 are analyzed below in detail.

1) Analysis of radiation Null 1

Firstly, to illustrate the mechanism of radiation null 1 at around 32 GHz, a simple transmission-line equivalent circuit is depicted in Fig. 5. The driven patch section is represented as an open-circuited transmission line. The parasitic patches are represented as two transmission line (one pair parasitic patches are represented one transmission line) with a gap between them. The gap is modelled by a π-network circuit, where C_s and C_p are the equivalent series gap capacitance and shunt gap capacitance of the radiating gap. Two fringing capacitances C_e are connected between the ends of the driven patch and the parasitic patches. In this model, all the radiation resistances of each section have been sum up to one resistor. Due to the differential fed method, an equivalent electric wall at the central line divides this model into two identical sections. Accordingly, a shunt series resonant circuit can be extracted from the parasitic patches which is marked with red-dashed rectangle circle. The impedance Z_{n1} of the circuit can be given by (1)

$$Z_{n1} = Z_p \frac{\frac{1}{j\omega C_C} + jZ_p \tan\theta_p}{Z_p + \frac{\tan\theta_p}{\omega C_C}} + \frac{1}{j\omega C_e} \tag{1}$$

This article has been accepted for publication in a future issue of this journal, but has not been fully edited. Content may change prior to final publication. Citation information: DOI 10.1109/TAP.2020.2975534, IEEE Transactions on Antennas and Propagation

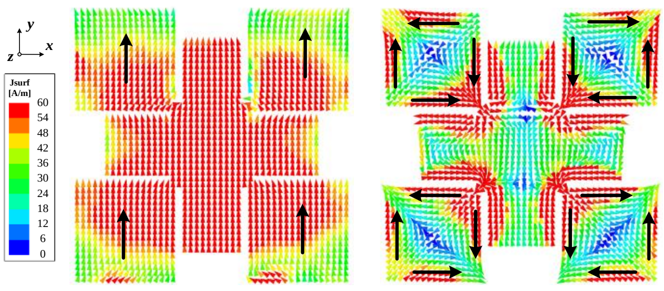

(a) (b)

Fig. 7. The surface current distributions on the driven patch of reference Design II at (a) the central operating frequency 27 GHz and (b) the frequency 22 GHz of Null 2.

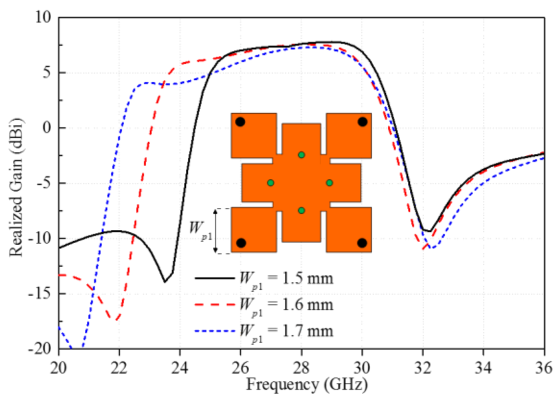

Fig. 8. Simulated realized gains of reference Design II for different W_{p1}.

where ω is the angular frequency, Z_p is the characteristic impedance of one pair parasitic patches, $\theta_p = \beta W_p$ denotes the electric length of one pair parasitic patches and the capacitor $C_c = 2C_s + C_p$. Obviously, a series resonance can be obtained with the condition $Z_{n1} = 0$ which can be approximately written as (2) if $Z_p\omega \gg 1$.

$$\theta_p = \arctan\frac{(C_c + C_e)Z_p\omega}{Z_p^2\omega^2 C_c C_e - 1} \approx \arctan\frac{C_c + C_e}{Z_p\omega C_c C_e} \tag{2}$$

On this condition, the parasitic patches can be equivalent to be a bandstop circuit and thus generate radiation Null 1. The frequency of Null 1 is given as

$$f_{Null1} = \frac{1}{2\pi Z_p \tan\theta_p}\left(\frac{1}{C_c} + \frac{1}{C_e}\right) \tag{3}$$

According to (3), Null 1 can be independently tuned by the slot width W_s (which controls the central capacitor C_s). As observed in Fig. 6, Null 1 shifts clearly from 30.5 to 32.5 GHz while W_s is increased from 0.1 to 0.3 mm. This is reasonable because the central capacitor C_s is decreased.

2) Analysis of radiation Null 2

Next, to investigate the generative mechanism of Null 2, the current distribution on the driven patch of reference Design II is illustrated in Fig 7. As a contrast, the current distribution at the central operating frequency 27 GHz is first depicted in Fig. 7(a). It can be seen that the current mainly concentrates on the center of the cross-shaped patch, leading to efficient radiation at 27 GHz. While at the frequency 22 GHz of Null 2, as shown in Fig. 7(b), less current distributes on the center of the cross-shaped driven patch and most of the current is confined around the shorted patches. In addition, the current path along the two perpendicular sides of each shorted patch exhibits a half-wavelength resonance, thus generating the radiation null.

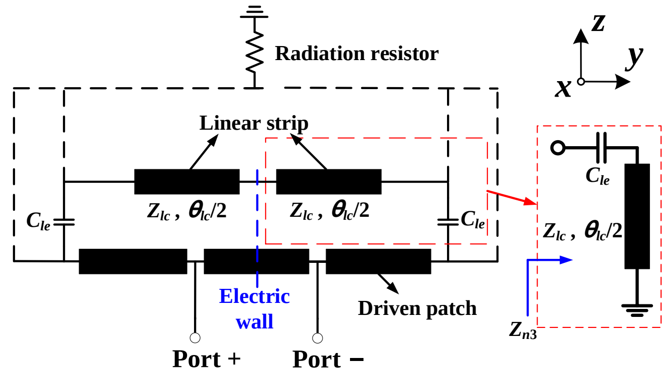

Fig. 9. The equivalent circuit model for reference Design III.

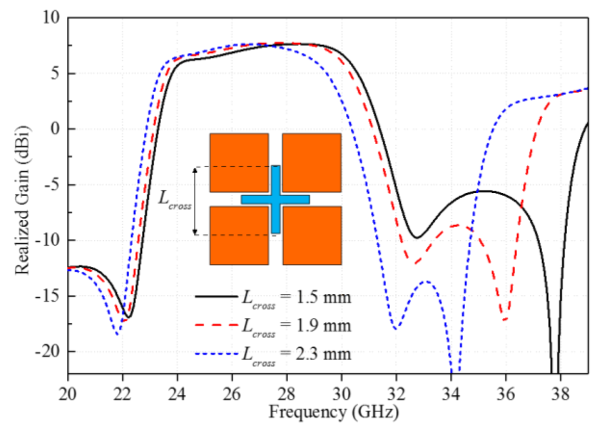

Fig. 10. Simulated realized gains of reference Design III for different L_{cross}.

Fig. 8 shows the tuning of Null 2. It can be observed that the frequency of Null 2 shifts from 23.75 to 20.5 GHz while W_{p1} increases from 1.5 to 1.7 mm. This is reasonable because the current length along the edges of each shorted patch is increased. Therefore, by tuning the sizes of the shorted patches, Null 2 can be individually controlled, and the frequency can be estimated by (4).

$$f_{Null2} = \frac{c}{4W_{p1}\sqrt{\varepsilon_{eff}}} \tag{4}$$

where c is the speed of light in vacuum, ε_{eff} represents the effective dielectric constant of the substrate.

3) Analysis of radiation Null 3

Then, to demonstrate the mechanism of radiation Null 3 in reference Design III, a transmission-line equivalent circuit can be given in Fig. 9. The cross strip is represented as an open-circuited transmission line (the influence of parasitic patches is eliminated for brevity). Two fringing capacitances C_{le} are connected between the ends of the driven patch and the cross strip. Accordingly, a shunt series resonant circuit can be approximately extracted from the linear strip marked with red-dashed rectangle circle. The impedance Z_{n3} can be given by (5)

$$Z_{n3} = jZ_{lc}\tan\frac{\theta_{lc}}{2} + \frac{1}{j\omega C_{le}} \tag{5}$$

This article has been accepted for publication in a future issue of this journal, but has not been fully edited. Content may change prior to final publication. Citation information: DOI 10.1109/TAP.2020.2975534, IEEE Transactions on Antennas and Propagation

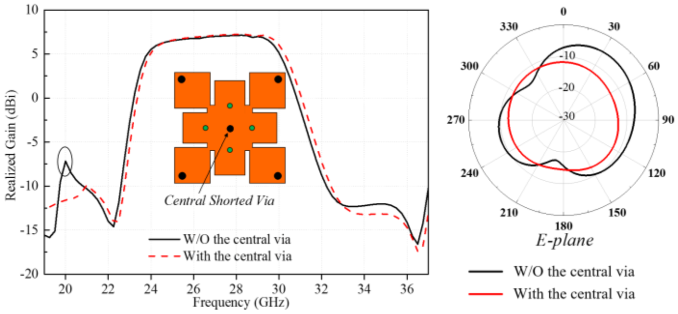

(a) (b)

Fig. 11. (a) Simulated realized gains of the proposed antenna. (b) Simulated patterns of the proposed antenna at 20 GHz.

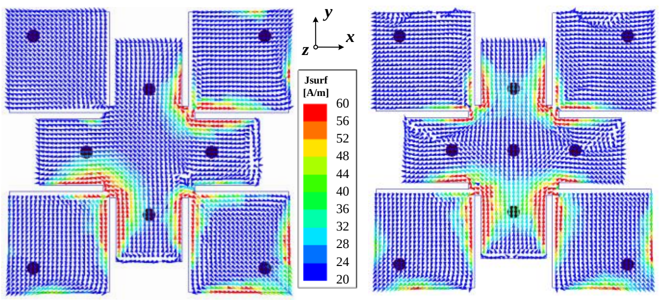

(a) (b)

Fig. 12. The current distribution on the driven patch of the proposed antenna at the weak resonant frequency 20 GHz. (a) Without the central via. (b) With the central via.

where ω is the angular frequency, Z_{lc} is the characteristic impedance of the linear strip, $\theta_{lc} = \beta L_{cross}$ denotes the electric length of the linear strip. Also, if the fringing capacitance C_{le} is negligible or $\omega C_{le} \ll 1$, the condition $Z_{n3} = 0$ can be simplified as

$$\theta_{lc}=2\pi\sqrt{\varepsilon_{eff}}\,\frac{L_{cross}}{\lambda_{Null3}}\approx\pi \tag{6}$$

Then the resonance frequency can be given by

$$f_{Null3}=\frac{c}{2L_{cross}\sqrt{\varepsilon_{eff}}} \tag{7}$$

At the resonant frequency, the cross strip is equivalent to a bandstop circuit thus suppressing the radiation of the driven patch. According to (7), radiation Null 3 can be controlled by the length of the linear strip L_{cross}. As observed in Fig. 10, Null 3 shifts clearly from 38 to 34 GHz while L_{cross} is increased from 1.5 to 2.3 mm.

C. The effect of the central shorting via

Finally, the differential networks are added to reference Design III, and the proposed antenna is obtained. However, it is found that the rejection level of the lower stopband deteriorates at around 20 GHz because of a weak resonance, as shown in Fig. 11 (see the black solid line). To solve this problem, a shorting via is loaded at the central point of the driven patch. With reference to the red dash line in Fig. 11(a), the weak resonance is suppressed and the rejection level at 20 GHz is improved. Also, the radiation pattern shrinks overall at 20 GHz with the central via loaded. In order to illustrate this phenomenon, the current distributions on the driven patch are shown in Fig. 12. It can be seen that without the central via, the current distribution is asymmetry because the phase difference of the differential feeding network is no longer 180 degrees but only about 100 degrees. When adding the central via, a relatively symmetrical current distribution is obtained, as shown in Fig. 12(b). In this case, more current is confined to the four slots between the cross-shaped patch and the shorted patches. Consequently, a better suppression is achieved at 20 GHz.

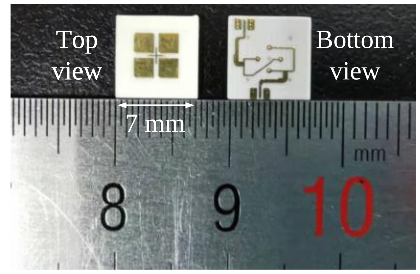

Fig. 13. Prototype of the proposed dual-polarized filtering antenna.

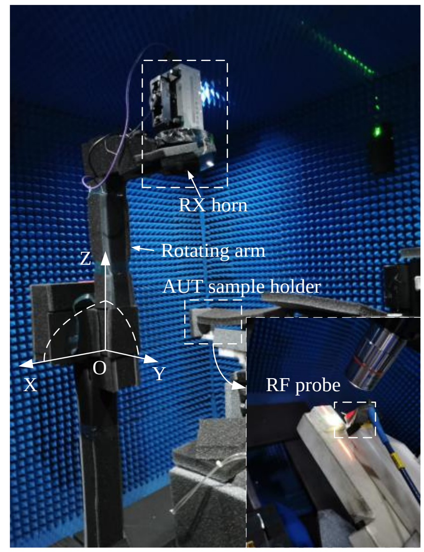

Fig. 14. The antenna measurement setup.

III. Antenna Implementation

A. Design Guideline

Base on the above discussions, a design guideline for the dual-polarized filtering patch antenna is summarized as follows.

1) Firstly, use four square planar parasitic patches and a cross-shaped driven patch to design a differential-fed dual-polarized stacked patch antenna. Set the initial dimension of the driven patch as $0.5 \times 0.5\ \lambda_0^2$ (λ_0 denotes the guided wavelength in the substrate at the central frequency of the passband). In addition, set the initial side-length of each parasitic patch as $0.25\lambda_0$.
2) Secondly, tune the width (W_{s1}) of the slot between the four parasitic patches to adjust the first desired upper-stopband radiation null.
3) Thirdly, add four shorted patches into the inner corners of the cross-shaped driven patch. Set the initial side-length of each shorted patch as $0.25\lambda_{Null2}$ (λ_{Null2} denotes the guided wavelength in the substrate at the frequency of the desired

This article has been accepted for publication in a future issue of this journal, but has not been fully edited. Content may change prior to final publication. Citation information: DOI 10.1109/TAP.2020.2975534, IEEE Transactions on Antennas and Propagation

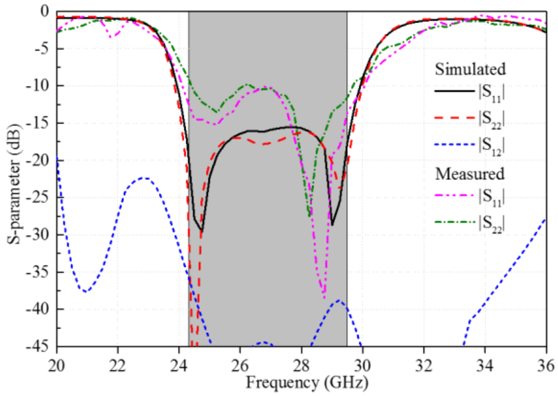

(a)

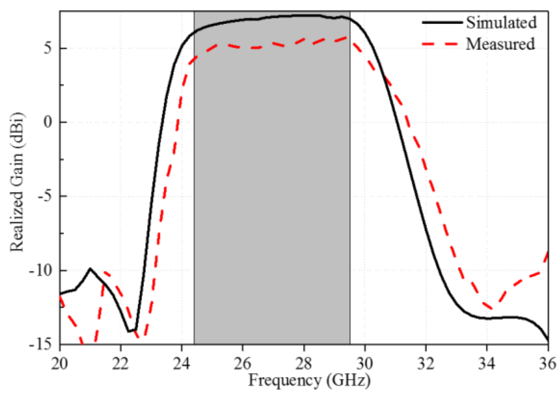

(b)

Fig. 15. (a) Simulated and measured S-parameters of the prototype. (b) Simulated and measured realized gains of the prototype.

lower stopband radiation null), and tune it to obtain the desired lower stopband radiation null.

4) Fourthly, introduce a cross-shaped strip between the four parasitic patches. Set the initial length of the cross-shaped strip as $0.5\lambda_{Null3}$ (λ_{Null3} denotes the guided wavelength in the substrate at the frequency of the second desired upper-stopband radiation null), and tune it to obtain the desired second desired upper-stopband radiation null.
5) Finally, refine each parameter to optimize the design for obtaining good impedance matching and required bandwidth.

B. *Experiment*

For verification, the proposed multilayer dual-polarized filtering patch antenna is designed and fabricated with the standard PCB process. The fabricated prototype photograph is demonstrated in Fig. 13. It should be mentioned that in this design, the coplanar waveguide (CPW) feeding structure is employed to adapt to the prospective RFIC connection. Fig. 14 shows the antenna measurement setup. The Cascade Microtech ground-signal-ground (GSG) RF probe with 450 um pitch is used to contact the CPW line feeding port, and only one port can be tested at a time, which means the measurement of $|S_{21}|$ is not realizable. A rotating arm with RX horn antenna is used to measure the radiation patterns of the prototype. However, the testing angle in the YoZ plane is limited to the range of 0 − 230 degrees because that the rotating arm is blocked by the AUT sample holder. Therefore, the measured radiation patterns in this plane is not complete and the results in the range of 230 − 360 degrees are not obtainable.

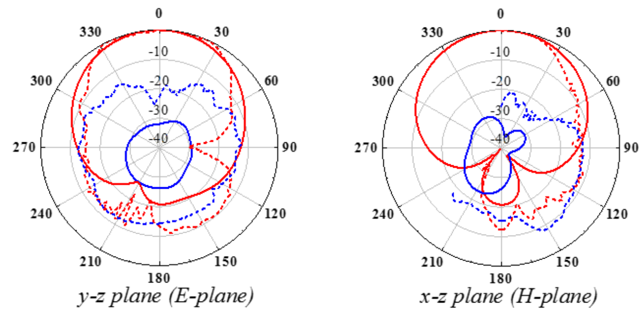

(a)

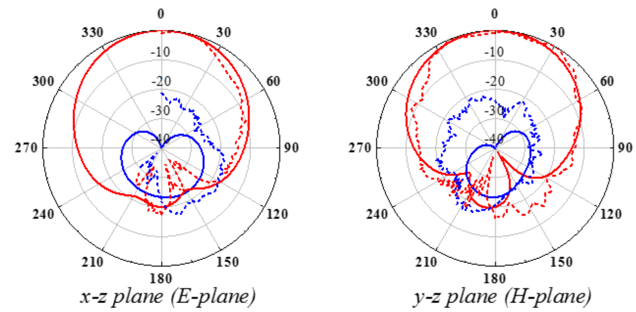

(b)

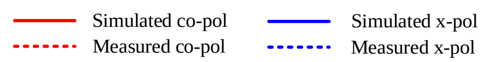

Fig. 16. Simulated and measured patterns of the prototype. (a) Port 1. (b) Port 2.

The simulated and measured S-parameters of the two ports are illustrated in Fig. 15(a), showing good agreement. As observed, the center operating frequency of this antenna is 27 GHz and the impedance bandwidths ($|S_{11}| < -10$ dB) measured at both ports are 20% (24.25−29.5 GHz). In addition, the simulated $|S_{21}|$ is lower than −35 dB across the entire passband.

The simulated and measured boresight gains are shown in Fig. 15(b). With reference to the figure, the average measured in-band gain is 5.2 dBi, while the average simulated in-band gain is 6.6 dBi. The gain reduction between the simulated and measured results are mainly due to the following factors: 1) the insertion loss of the RF probe; 2) the uncertainty of the material property at 27 GHz; 3) the resistive losses of the metallic vias; 4) the fabrication and measurement errors. The gain drops quickly to below −10 dB at 23 GHz and 33 GHz respectively, which exhibits sharp roll-off rates at the upper and lower band-edges. In the stopband, the radiation suppression level is 16 dB in simulation and 13 dB in measurement. Owing to the symmetry of the structure, the realized gains of the two ports are nearly the same with each other, which is to be expected.

Fig. 16 shows the measured and simulated radiation patterns of the dual-polarized prototype at the central frequency 27 GHz. Similar broadside radiation patterns are obtained at both ports, as expected. At the boresight direction, the co-polarized fields are stronger than the cross-polarized counterparts by more than 30 dB in simulation and 20 dB in measurement. Besides, the simulated and measured 3-dB HPBWs are 75° and 76° in the E-plane, while given by 78° and 82° in the H-plane. The patterns at other frequencies have also been studied, and they

This article has been accepted for publication in a future issue of this journal, but has not been fully edited. Content may change prior to final publication. Citation information: DOI 10.1109/TAP.2020.2975534, IEEE Transactions on Antennas and Propagation

TABLE II
COMPARISON WITH THE PREVIOUS MILLIMETER-WAVE FILTERING ANTENNAS

Ref.	**Antenna type**	**Polarization**	**Imp. BW (|S11|< −10dB)**	**Ave. gain (dBi)**	**Extra filtering circuit**	**Controllable radiation null**	**Process technology**	**Overall size (λ_c^3)/ Radiator size of each element (λ_c^2)**
[12] SIW	Single element	Single	1.56% (31.25−31.75GHz)	6.7	Yes	2	Standard PCB	0.92×1×0.092/ 0.56×0.61
[13] SIW	1×4 subarray	Single	1.2% (28.9−29.6GHz)	8.1	Yes	0	Standard PCB	2.1×1.67×0.085/ 0.44×0.92
[11] Patch	1×4 subarray	Single	5% (27.15−28.55GHz)	11.1	Yes	0	Standard PCB	3.1×2.5×0.12/ 0.26×0.2
[24] Aperture	2×2 subarray	Single	2.94% (33.5−34.5GHz)	12.5	Yes	0	3-D printing	1.46×1.46×1.5/ 0.57×0.4
[14] SIW	2×2 subarray	Dual	1.6% (36.7−37.3GHz)	10.8	Yes	0	LTCC	1.73×1.73×0.24/ 0.58×0.58
This work	Single element	Dual	20% (24.25−29.5GHz)	5.2	No	3	Standard PCB	0.63×0.63×0.09/ 0.4×0.4

are found quite stable across the entire passband.

C. Comparison

To address the advantages of the proposed design, a comparison with the previous mm-Wave filtering antennas is tabulated in Table II. It can be observed that the proposed filtering antenna possesses a much wider impedance bandwidth (20%) than the existing mm-Wave filtering antennas (1.56% in [12], 1.2% in [13], 5% in [11], 2.94% in [24] and 1.6% in [14]). In addition, a more compact size is achieved in the proposed antenna (the overall size of the proposed antenna is 0.63 ×0.63 ×0.089 λ_c^3, and the size of the radiating patches is 0.4 ×0.4 λ_c^2), which is more suitable for array applications. Most importantly, it should be mentioned that three radiation nulls can be independently controlled by tuning respective parameters of the proposed antenna, without requiring extra filtering circuit. Therefore, the proposed dual-polarized antenna is able to reduce the cost and space of the RF frontend system.

IV. CONCLUSION

In this paper, a novel dual-polarized filtering antenna operating in the 5G mm-Wave band (24.25−29.5 GHz) has been investigated. The generative mechanism of the filtering response has been studied. It has been shown that three radiation nulls can be introduced and individually tuned just by properly designing the parameters of the antenna, exhibiting high design freedom. With standard PCB process, a low-cost prototype has been fabricated and tested. The prototype shows a compact size, a wide bandwidth and a sharp roll-off rate at the edge of passband. These merits make the proposed antenna a good candidate as an element for 5G mm-Wave massive-MIMO applications.

REFERENCES

[1] J. Zhang, X. Ge, Q. Li, M. Guizani, and Y. Zhang, “5G millimeter-wave antenna array: design and challenges,” *IEEE Wireless Commun*., Oct. 2016, doi: 10.1109/MWC.2016.1400374RP.

[2] M. G. Bautista, H. Zhu, X. Zhu, Y. Yang, Y.-C. Sun and E. Dutkiewicz, “Compact millimeter-wave bandpass filters using quasi-lumped elements in 0.13-um (Bi)-CMOS technology for 5G wireless systems,” *IEEE Trans. Microw. Theory Techn.*, vol. 67, no. 7, pp. 3064-3073, Jul. 2019.

[3] H. Zhu, X. Zhu, Y. Yang and Q. Xue, “Design of wideband third-order bandpass filters using broadside-coupled resonators in 0.13-um (Bi)-CMOS technology,” *IEEE Trans. Microw. Theory Techn.*, vol. 66, no. 12, pp. 5593-5604, Dec. 2018.

[4] C.-L. Yang, C.-Y. Shu and Y.-C. Chiang, “Design of a K-band chip filter with three tunable transmission zeros using a standard 0.13-um CMOS technology,” *IEEE Trans. Circuits Syst. II, Exp. Briefs*., vol. 57, no. 7, pp. 522–526, Jul. 2010.

[5] M. Stickel, P. Kremer and G. V. Eleftheriades, “A millimeter-wave bandpass waveguide filter using a width-stacked silicon bulk micromachining approach,” *IEEE Microw. Compon. Lett*., vol. 16, no. 4, pp. 209–211, Apr. 2006.

[6] J. A. Martinez, J. J. de Dios, A. Belenguer, H. Esteban and V. E. Boria, “Integration of a very high quality factor filter in empty substrate-integrated waveguide at Q-band,” *IEEE Microw. Compon. Lett*., vol. 28, no. 6, pp. 503–505, Jun. 2018.

[7] M.-C. Tang, Y. Chen, and R. W. Ziolkowski, “ Experimentally validated, planar, wideband, electrically small, monopole filtennas based on capacitively loaded loop resonators”, *IEEE Trans. Antennas Propag.*, vol.64, no. 8, pp. 3353-3360, Aug. 2016.

[8] M.-C. Tang, Z. Wen, H. Wang, M. Li and R. W. Ziolkowski, “Compact, frequency-reconfigurable filtenna with sharply defined wideband and continuously tunable narrowband states”, *IEEE Trans. Antennas Propag.*, vol.65, no. 10, pp. 5026-5034, Oct. 2017.

[9] C.-X. Mao, S. Gao, Y. Wang, Z.-P. Wang, F. Qin, B.-S. Izquierdo, and Q.-X. Chu, “An integrated filtering antenna array with high selectivity and harmonic suppression,” *IEEE Trans. Microw. Theory Techn.*, vol. 64, no. 6, pp. 1798-1805, Jun. 2016.

[10] C.-X. Mao, S. Gao, Y. Wang, Q. Luo and Q.-X. Chu, “A shared-aperture dual-band dual-polarized filtering-antenna-array with improved frequency response,” *IEEE Trans. Antennas Propag.*, vol. 65, no. 4, pp. 1836-1844, Apr. 2017

[11] H.-Y. Jin, G.-Q. Luo, W.-L. Wang, W.-Q. Che and K.-S. Chin, “Integration design of millimeter-wave filtering patch antenna array with SIW four-way anti-phase filtering power divider,” *IEEE Access*., accepted for publication.

[12] H. Chu, C. Jin, J.-X. Chen, and Y.-X. Guo, “A 3-D millimeter-wave filtering antenna with high selectivity and low cross-polarization,” *IEEE Trans. Antennas Propag.*, vol. 63, no. 5, pp. 2375-2380, May 2015.

[13] H. Chu, J.-X. Chen, S. Luo, and Y.-X. Guo, “A millimeter-wave filtering monopulse antenna array based on substrate integrated waveguide technology,” *IEEE Trans. Antennas Propag.*, vol. 64, no. 1, pp. 316-321, Jan. 2016.

[14] H. Chu and Y.-X. Guo, “A filtering dual-polarized antenna subarray targeting for base stations in millimeter-wave 5G wireless communications,” *IEEE Trans. Compon., Packag., Manuf. Technol*., vol. 7, no. 6, pp. 964-973, Jun. 2017.

[15] X. Y Zhang, W. Duan, and Y-M. Pan, “High-gain filtering patch antenna without extra circuit,” *IEEE Trans. Antennas Propag.*, vol.63, no.12, pp. 5883-5888, Dec. 2015.

[16] J.-F. Qian, F.-C. Chen, Q.-X Chu, Q. Xue and Michael J. Lancaster, “A novel electric and magnetic gap-coupled broadband patch antenna with improved selectivity and its application in MIMO system,” *IEEE Trans. Antennas Propag.*, vol.66, no.10, pp. 5625-5629, Oct. 2018.

[17] W. Duan, X. Y. Zhang, Y.-M. Pan, J.-X. Xu and Q. Xue, "Dual-polarized filtering antenna with high selectivity and low cross polarization," *IEEE Trans. Antennas Propag*., vol. 64, no. 10, pp. 4188−4196, Oct. 2016.
[18] J.-Y. Jin, S.-W. Liao, and Quan Xue, "Design of filtering-radiating patch antennas with tunable radiation nulls for high selectivity," *IEEE Trans. Antennas Propag*., vol. 66, no. 4, pp. 2125−2130, April. 2018.
[19] W.-C. Yang, M.-Z. Xun,W.-Q. Che, W.-J. Feng, Y.-Q. Zhang and Q. Xue, "Novel compact high-gain differential-fed dual-polarized filtering patch antenna," *IEEE Trans. Antennas Propag*., accepted for publication.
[20] S.-J. Yang, Y.-M. Pan, Y. Zhang, Y. Gao and X. Y. Zhang, "Low-profile dual-polarized filtering magneto-electric dipole antenna for 5G applications," *IEEE Trans. Antennas Propag.*, accepted for publication.
[21] T.-L. Wu, Y.-M. Pan, P.-F. Hu and S.-Y. Zheng, "Design of a low profile and compact omnidirectional filtering patch antenna," *IEEE Access*., vol.5, pp. 1083-1089, March. 2017.
[22] Y.-M. Pan, P.-F. Hu, K. W. Leung, and X. Y. Zhang, "Compact single-/dual-polarized filtering dielectric resonator antennas," *IEEE Trans. Antennas Propag.*, vol. 66, no. 9, pp. 4474−4484, Sep. 2018.
[23] C.-F. Ding, X. Y. Zhang, Y. Zhang, Y.-M. Pan and Q. Xue, "Compact broadband dual-polarized filtering dipole antenna with high selectivity for base station applications," *IEEE Trans. Antennas Propag.*, vol. 66, no. 11, pp. 5747-5756, Nov. 2018.
[24] X. He, Y. Zhang, M. Du and J. Xu, "Lightweight and compact high-gain filtering aperture antenna fabricated by three-dimensional printing technology," *IEEE Antennas Wireless Propag. Lett*., vol. 17, no.7, pp. 1141–1144, July. 2018

Sheng Jie Yang was born in Hunan, China. He is now pursuing the PhD degree at School of Electronic and Information Engineering, South China University of Technology, Guangzhou, China.

His current research interests focus on filtering antennas, millimeter-wave antennas, and base station antennas.

Yong Mei Pan (M'11−SM'17) was born in Huangshan, Anhui Province, China. She received the B.Sc. and Ph.D. degrees in electrical engineering from the University of Science and Technology of China, Hefei, China, in 2004 and 2009, respectively. From 2009 to 2012, she was a Research Fellow with the Department of Electronic Engineering, City University of Hong Kong, Kowloon Tong, Hong Kong. In 2013, she joined the School of Electronic and Information Engineering, South China University of Technology (SCUT), Guangzhou, China, as an Associate Professor. Currently, she is a Professor with SCUT. Her research interests include dielectric resonator antennas, leaky wave antennas, metasurface antennas, and filtering antennas.

Prof. Pan is now an Associate Editor of the *IEEE Transactions on Antennas and Propagation*.

Xiu Yin Zhang (S'07-M'10- SM'12) received the B. S. degree in communication engineering from Chongqing University of Posts and Telecommunications, Chongqing, China, in 2001, the M.S. degree in electronic engineering from South China University of Technology, Guangzhou, China, in 2006, and the PhD degree in electronic engineering from City University of Hong Kong, Kowloon, Hong Kong, in 2009.

From 2001 to 2003, he was with ZTE Corporation, Shenzhen, China. He was a Research Assistant from July 2006 to June 2007 and a Research Fellow from September 2009 to February 2010 with the City University of Hong Kong. He is currently a full professor and vice dean with the School of Electronic and Information Engineering, South China University of Technology. He also serves as the vice director of Guangdong key laboratory of millimeter-wave and terahertz and the vice director of the Engineering Research Center for Short-Distance Wireless Communications and Network, Ministry of Education. He has authored or coauthored more than 140 internationally referred journal papers (including more than 80 IEEE Transactions) and around 80 conference papers. His research interests include antennas and arrays, MMIC, microwave/terahertz circuits and sub-systems, and wireless communications.

Dr. Zhang is a Fellow of the Institution of Engineering and Technology. He has served as General chair/Technical Program Committee (TPC) chair/ member and Session Organizer/Chair for a number of conferences. He was a recipient of the National Science Foundation for Distinguished Young Scholars of China, the Leading Talent of Technological Innovation of Ten-Thousands Talents Program, the Young Scholar of the Changjiang Scholars Program of Chinese Ministry of Education. He was a recipient of the Scientific and Technological Award (First Honor) of Guangdong Province. He was the supervisor of several conference best paper award winners.